Regional budgets for nitrogen oxides from continental sources: Variations of rates for oxidation and deposition with season and distance from source regions

J. William Munger, Song-Miao Fan,[1] Peter S. Bakwin,[2] Mike L. Goulden,[3]
Allen. H. Goldstein,[4] Albert S. Colman,[5] and Steven C. Wofsy

Division of Engineering and Applied Sciences and Department of Earth and Planetary Sciences,
Harvard University, Cambridge, Massachusetts

[1] Now at Atmospheric & Oceanic Sciences Program, Princeton University, Princeton, New Jersey.
[2] Now at Climate Monitoring and Diagnostics Laboratory, National Oceanic and Atmospheric Administration, Boulder, Colorado.
[3] Now at Department of Earth System Science, University of California, Irvine, Irvine.
[4] Now at Department of Environmental Science, Policy, and Management, University of California, Berkeley.
[5] Now at Department of Geology and Geophysics, Yale University, New Haven Connecticut.

Abstract. Measurements of nitrogen deposition and concentrations of NO, NO_2, NO_y (total oxidized N), and O_3 have been made at Harvard Forest in central Massachusetts since 1990 to define the atmospheric budget for reactive N near a major source region. Total (wet plus dry) reactive N deposition for the period 1990-1996 averaged 47 mmol m^{-2} yr^{-1} (126 μmol m^{-2} d^{-1}, 6.4 kg N ha^{-1} yr^{-1}), with 34% contributed by dry deposition. Atmospheric input adds about 12% to the N made available annually by mineralization in the forest soil. The corresponding deposition rate at a distant site, Schefferville, Quebec, was 20 mmol m^{-2} d^{-1} during summer 1990. Both heterogeneous and homogeneous reactions efficiently convert NO_x to HNO_3 in the boundary layer. HNO_3 is subsequently removed rapidly by either dry deposition or precipitation. The characteristic (*e*-folding) time for NO_x oxidation ranges from 0.30 days in summer, when OH radical is abundant, to ~1.5 days in the winter, when heterogeneous reactions are dominant and O_3 concentrations are lowest. The characteristic time for removal of NO_x oxidation products (defined as NO_y minus NO_x) from the boundary layer by wet and dry deposition is ~1 day, except in winter when it decreases to 0.6 day. Biogenic hydrocarbons contribute to N deposition through formation of organic nitrates but are also precursors of reservoir species, such as peroxyacetylnitrate, that may be exported from the region. A simple model assuming pseudo first-order rates for oxidation of NO_x, followed by deposition, predicts that 45% of NO_x in the northeastern U.S. boundary layer is removed in 1 day during summer and 27% is removed in winter. It takes 3.5 and 5 days for 95% removal in summer and winter, respectively.

1. Introduction

Human activities have greatly increased the inputs of nitrogen oxides to the atmosphere (we define nitrogen oxides as follows: NO_x = NO + NO_2, radicals that rapidly interconvert, within minutes to hours; and NO_y = NO_x + NO_3 + N_2O_5 + HNO_3 + peroxyacetylnitrate (PAN) + other organic nitrates + aerosol nitrate, the family of radicals and nonradicals that interconvert and are deposited on longer timescales *i.e.*, hours to days) [*Davidson,* 1991*; Galloway et al*., 1995; *Logan,* 1983; *Prather et al*., 1995]. Anthropogenic emissions of NO_x (mainly from combustion) exceed the natural inputs of fixed nitrogen to the atmosphere in North America and other urbanized regions. Photochemical production of O_3 in the troposphere is controlled by NO_x radicals. Deposition of NO_y (along with NH_3) contributes to nutrient loading and acidification in sensitive ecosystems. Remote regions with low inputs from natural NO_x sources may be especially sensitive to even small increases in reactive N because chemical and ecological effects are nonlinear functions of concentration [*Liu et al.,* 1987*; Wedin and Tilman,* 1996]. The lifetime for NO_y removal determines the distance from the source region over which N levels are perturbed from the natural background. *Holland et al.* [1997] note that uncertainties in predicted global distri-

bution of nitrogen deposition lead to large differences in estimates of global carbon uptake associated with N fertilization.

Dentener and Crutzen [1993] noted the absence of a strong seasonality in wet deposition of NO_3^- over Europe and North America and argued that rates for production and removal of HNO_3 from the boundary layer are similar throughout the year, with increased rates of HNO_3 formation by heterogeneous hydrolysis of N_2O_5 in winter compensating for reduced rates of homogeneous oxidation of NO_2 by OH. However, the contribution from dry deposition was not included, and seasonal trends in wet deposition alone may be misleading. Total annual nitrate deposition fluxes have been estimated at sites in North America by inferring the dry deposition from average concentrations [*Hanson and Lindberg*, 1991; *Johnson and Lindberg*, 1992; *Meyers et al*., 1991], but long-term records of NO_x and NO_y concentrations and total (wet plus dry) nitrogen deposition fluxes have not been available to define seasonal cycles in the reactive nitrogen budget.

In 1990 we began continuous measurements of concentrations and eddy-covariance fluxes of NO_y, concentrations of NO_x and O_3, and deposition of NO_3^- in precipitation at Harvard Forest in central Massachusetts. Additional measurements were made during the Arctic Boundary Layer Expedition (ABLE 3B) experiment in the summer of 1990 near Schefferville, Quebec, *Munger et al*. [1996] (hereinafter referred to as M96) demonstrated that NO_y eddy fluxes can be reliably determined for extended periods by eddy-covariance measurements, identified horizontal and vertical transport and chemical reaction as dominant processes controlling dry deposition of NO_y to the forest canopy, and noted the absence of stomatal influence on NO_y dry deposition. In this paper we examine the seasonal trends in total nitrogen deposition, evaluate the mean lifetimes for oxidation of NO_2 and deposition of NO_y in the boundary layer, and estimate the rate of nitrogen removal during transport from source regions for the period 1990 through 1996.

2. Site Description and Measurement Methods

Harvard Forest is located in Petersham, Massachusetts (42.53°N, 72.18°W), at an elevation of 340 m. Within 100 km the surroundings are largely rural with a mix of mostly small (population of ~10^4) and a few medium (population of ~10^5) towns surrounded by forests. Extensive urban areas with relatively high NO_x emission densities lie within 200-500 km to the southwest of Harvard Forest (Figure 1). Average NO_x emissions given in the National Acid Precipitation Assessment Program (NAPAP) inventory within 250 km of Harvard Forest are 214 μmol m^{-2} d^{-1} [*Environmental Protection Agency (EPA)*, 1989], ranging from 417 μmol m^{-2} d^{-1} in the southwest quadrant, which includes the New York metropolitan area, to 75 μmol m^{-2} d^{-1} in the mostly rural northwest quadrant. The Boston metropolitan area is 100 km to the east; however, the prevailing winds are westerly, and emissions from Boston rarely reach the site. Harvard Forest is similar in many respects to much of the northeastern United States outside the urban corridor along the coast.

The ABLE 3B tower site was located 13 km NW of Schefferville, Quebec, Canada (54.83°N, 66.67°W), at an elevation of 500 m. Observations were made from mid-June to mid-August 1990. Besides Schefferville (largely abandoned and being demolished) and a few small villages the nearest habitations were >200 kilometers away. Schefferville is hundreds of km from major NO_x sources, except when forest fires are burning nearby; it represents a remote receptor site several days' transport time from major sources of NO_x , in contrast to Harvard Forest, which is immediately adjacent to a major source region.

Concentrations of NO were measured by using O_3 chemiluminescence. Concentrations of NO_2 and NO_y, respectively, were measured by using Xe-lamp photolysis and catalysis by hot Au with H_2, to convert NO_2 and NO_y to NO. Dry deposition fluxes of NO_y were determined by eddy covariance. Concentrations of O_3 at eight heights in the forest were determined by UV absorbance. Concentrations and fluxes of O_3 above the canopy were determined by using a fast-response C_2H_4-chemiluminescent analyzer. Full details of the measurements are given by M96.

At both sites, precipitation was collected above the canopy in a polyethylene funnel that opened only during precipitation events. The sample drained to a fractionating collector housed in a refrigerator. Concentrations of NO_3^-, SO_4^{2-}, and Cl^- were determined by ion chromatography. The analytical precision for rainwater analyses, determined from replicate analysis of samples and standards, was 2% or better. Additional data on precipitation composition at the National Atmospheric Deposition Program (NADP) Quabbin Reservoir site (42.392°N, 72.345°W) were obtained from the NADP data archive (http://nadp.nrel.colostate.edu/NADP/, National Atmospheric Deposition Program (NRSP-3)/National Trends Network, August, 1997, NADP/NTN Coord. Off., Ill. State Wat. Surv., Champaign, Ill., hereinafter referred to as NADP, 1997). Wet-deposition fluxes at Harvard Forest were corrected for missed samples or inefficient collection by multiplying the amount of precipitation recorded at a standard gauge located about 1 km from the tower (R. Lent, unpublished Harvard Forest data archives, 1997) by the volume-weighted average concentration for the event (for undersampled events) or by the monthly volume-weighted average (for missed events). Fresh and recently fallen snow-core samples were collected above polyethylene sheets set out at several locations within ≈50 m radius prior to a snow event. At Schefferville, rain volumes collected by the fractionating collector were used to compute rainfall amounts because rainfall in the area was topographically influenced [*Fitzjarrald and Moore*, 1994] and the nearest standard rain gauge was some distance away. Collection efficiency for light misting rains accompanied by winds may be less than 100% for the precipitation funnel. When rain was reported at the site, but sample was partially lost (spill or collector malfunction), the average depth for the rain gauge network [*Fitzjarrald and Moore*, 1994] was used.

3. Results

3.1 Sampling Statistics

Inevitably, long-term data sets are incomplete, and the simple sum of all the data does not provide total flux over the sampling interval. Gaps occur as a result of routine instrument calibrations, periodic shutdowns, sensor malfunctions, and other problems (e.g., lightning strikes, and power failures). Individual observations may not be truly independent. Diel variations, synoptic patterns, and seasonal trends introduce autocorrelation into the data. For example, the lagged correlation of mean midday NO_y eddy fluxes is 0.25 for a 1 day lag and exceeds 0.1 for lags up to 40 days. These correlations must be properly accounted for in filling data gaps and aggregating the data to monthly, seasonal, and annual timescales [*Goulden et al.,* 1996a].

Hourly observations of NO_y eddy flux consist of a central population that fits a lognormal distribution with some low outliers, as illustrated by the July data from Harvard Forest (Figure 2,top). Other time periods show similar patterns but with different ranges and median values. Integrated daily fluxes at Harvard Forest for each month (illustrated for July) and for Schefferville also fit a lognormal distribution over the central portion of their range (Figure 2, bottom). NO_y eddy fluxes had a mean diel cycle with a morning maximum (M96); the period 1000 to 1200 contributed nearly 20% of the integrated daily eddy flux. We have aggregated the data in

monthly increments, consistent with observed autocorrelation, to provide a sufficient number of observations from each hour of the day to obtain accurate means and still resolve seasonal variations. Means are computed independently for each hour of the day, and the mean diel cycle is summed to give mean daily flux for each month. The median or geometric mean represents the central tendency of lognormally distributed data. However, we use the arithmetic mean here because it incorporates important contributions from infrequent high-deposition events that may provide a significant fraction of total deposition during an averaging interval.

Half the NO_y eddy flux input at Schefferville, and during the summers at Harvard Forest, was deposited in extreme events on 25% and 20% of the days, respectively. Increasing skewness and contribution from rare events leads to greater potential for sampling error from missed data. We therefore examined the uncertainty associated with missing data by generating random subsamples of the data. The means (or medians) of subsamples containing ≥50% of the data vary by 10-15%. Variability increases sharply as more data are excluded (Figure 3). We estimated the uncertainty of the NO_y eddy-flux totals by computing the standard deviation of random subsamples that include 50% of the data from each interval.

On account of the smaller sample size for Schefferville data, individual days were integrated separately. Missing data were interpolated between adjacent points; days with fewer than 20 hours of valid data were rejected, and daily totals were computed. These values were used to obtain a seasonal mean, and estimates of the sampling uncertainty were derived from the standard deviation of data from valid days.

3.2 Combined Deposition

3.2.1. Harvard Forest. Monthly average concentrations of NO_3^- in rainwater at Harvard Forest (Figure 4,top) compared closely with the long-term means for rain sampled at the nearby NADP Quabbin reservoir site, implying that precipitation collected at Harvard Forest is regionally representative. The annual volume-weighted mean concentration of NO_3^- at Harvard Forest was 25 μmol l^{-1}**,** with a minimum of ~20 μmol l^{-1} in fall and winter and a maximum of 30 μmol $^{-1}$ in early summer. Daily inputs of NO_3^- by precipitation ranged from <1 μmol m^{-2} d^{-1} for a trace of rain to >2000 μmol m^{-2} d^{-1} for a particularly dirty (NO_3^- = 100 μmol l^{-1}) large event. The distribution of wet-deposition data at Harvard Forest was highly skewed; 13% of the events with largest inputs contributed half the wet deposition of NO_3^-, a more significant influence of extreme events than that for dry deposition. Wet deposition of NO_3^- (Figure 4, bottom) peaked in summer at Harvard Forest, as observed at Quabbin Reservoir and other NADP sites in the northeastern United States (NADP, 1997).

Daily integrated NO_y eddy fluxes measured by eddy covariance ranged from near 0 to 470 μmol m^{-2} d^{-1}. Mean daily dry-deposition fluxes of NO_y at Harvard Forest for monthly intervals generally showed low values in winter and higher values in summer or fall (Figure 5). The integrated daily NO_y eddy fluxes show seasonal differences that were not observed in the midday mean eddy fluxes because of day length differences and the strong diel cycle in NO_y eddy fluxes during summer months (M96). Monthly deposition (wet plus dry) of reactive N for the 7 years beginning January 1, 1990 (Figure 6) exhibited values of around 200 μmol m^{-2} d^{-1} during the growing seasons of all years except 1995, which had an exceptional drought. Eddy fluxes (dry deposition) of N during the summer of 1990 were higher, and nitrate wet deposition was lower than that in subsequent years. Unusual meteorological conditions may be responsible, but possible artifacts from a change in the NO_y catalyst (M96) cannot be ruled out. Nevertheless, conclu-

sions drawn from the 7-year data set are not significantly different from the 6-year data set excluding 1990. Variations in wet inputs tended to compensate for changes in dry deposition. The decline in dry deposition during 1994 (Figure 5) was offset by increased wet deposition, and the total deposition (Figure 6) was comparable to previous years. However, reduced wet deposition during a severe drought in summer 1995 was not offset by increased dry deposition. Total NO_y inputs on an annual basis, averaged 47 ± 7.4 (sum of monthly means plus or minus monthly standard deviation) mmol m^{-2} yr^{-1} (Figure 7) with 34% contributed by dry deposition. Total reactive N deposition was highest in summer and early fall (4-5 mmol m^{-2} $month^{-1}$; 150 μmol m^{-2} d^{-1}) and decreased by about a factor of 2 in winter months. Peak deposition rates coincide with highest fraction of NO_x oxidation products (minima in NO_x :NO_y) and not with the maximum NO_y concentrations, which are highest in winter (M96).

3.2.2. Schefferville. The overall volume-weighted NO_3^- concentration in rainwater at the Schefferville tower site was 3.8 μmol l^{-1}, roughly a factor of 10 less than that at Harvard Forest in summer. Nitrate deposition in rainwater varied from 0.4 μmol m^{-2} d^{-1} to 120 μmol m^{-2} d^{-1}, with a mean and median of 15 and 7 μmol m^{-2} d^{-1}, respectively. Seven days (14%) of a total of 50 rainy days accounted for 50% of the NO_3^- wet deposition, indicating that sporadic advection of pollutants was very important. A single event with ~10 μmol l^{-1} [NO_3^-] on July 30, which has been identified as an anthropogenic pollution event [*Bakwin et al.*, 1994], contributed 17% of the wet deposition during the period.

Integrated daily NO_y eddy fluxes were 0.7-37 μmol $m^{-2}d^{-1}$ (*M96*, Figure 5), with a mean and median of 7.6 and 6.4 μmol m^{-2} d^{-1}, respectively. Dry-deposition fluxes of nitrate were more uniform than wet-deposition fluxes; daily totals exceeded 14 μmol m^{-2} d^{-1} on only 4 days (Figure 8). Total NO_y inputs ranged from <5 to 130 μmol m^{-2} d^{-1}, with a mean value of 18.5 μmol m^{-2} d^{-1} (0.55 mmol m^{-2} $month^{-1}$), about 12% of the deposition rate at Harvard Forest during summer. Dry deposition contributed 41% of the total reactive N deposition at the Schefferville site, compared to 77% during the same period at Harvard Forest. On average, however, dry deposition contributed 35% of the total reactive N deposited during summer at Harvard Forest.

3.3 Regional Comparisons

Deposition rates for N determined at 20 northeastern U.S. sites in the National Dry Deposition Network (NDDN) and the Integrated Forest Study (IFS) ranged from 24 to 68 mmol m^{-2} yr^{-1} (mean 43) [*Johnson and Lindberg,* 1992*; Meyers et al.*, 1991]. The deposition rates determined in these studies by inferential method are consistent with the eddy-covariance measurements at Harvard Forest. Estimated contributions from dry deposition at IFS and NDDN sites fell in the range 30-70%, which is comparable to results of direct measurements from Harvard Forest and Schefferville. Nitrogen deposition fluxes at Harvard Forest were intermediate between deposition at West Point, New York (56 mmol m^{-2} yr^{-1}) and Howland, Maine (34 mmol m^{-2} yr^{-1}), consistent with the southwest-to-northeast decline in N deposition across the region noted by *Ollinger et al.* [1993]. No clear seasonal cycle in total N deposition was apparent across the NDDN [*Meyers et al.*, 1991], although the West Point site in New York had a summer maximum during 2 of 3 years studied. The seasonal trends at Harvard Forest become most apparent when many years of data are aggregated; this finding illustrates the value of long-term data sets in identifying underlying patterns that may be masked by atmospheric variability (e.g. wet summer in 1991 and dry summer in 1990).

3.4 Ammonium Inputs

Reduced nitrogen in the form of NH_3 and NH_4^+ in precipitation and dry deposition also contributes biologically available N. We did not measure NH_4^+ in precipitation at Harvard Forest, but we can estimate it from the measured SO_4^{2-} inputs at Harvard Forest and mean NH_4^+:SO_4^{2-} ratio in precipitation collected at the Quabbin Reservoir NADP site (NADP, 1997) (Figure 9). Estimated wet deposition of NH_4^+ (8.1 mmol m^{-2} yr^{-1}) was ≈15% of the total NO_3^- input at Harvard Forest. *Tjepkema et al*. [1981] observed low concentrations and deposition of NH_3 at Harvard Forest and estimated that aerosol deposition of NH_4^+ added 4.3 mmol m^{-2} yr^{-1}. Recent measurements [*Lefer,* 1997] (B.L. Lefer et al., Nitric acid and ammonia at a rural northeastern U.S. site, submitted to *Journal of Geophysical Research,* 1997) confirm that NH_3 levels are low at Harvard Forest.

4. Discussion

4.1 Atmospheric Contribution to Ecosystem Nitrogen Pools

Atmospheric N deposition at Harvard Forest is significant in comparison with the N turnover by vegetation but small in relation to the total N content of vegetation and soils. Total N in the near-surface soil (5410 mmol m^{-2}) at a nearby hardwood stand [*Aber et al.,* 1993] represents about 90 years accumulation at present rates for nitrate plus ammonium deposition (60.4 mmol N m^{-2} yr^{-1}). Combined input of atmospheric nitrate and ammonium also appears small (~12%) in comparison with the annual net N mineralization rate of 500 mmol m^{-2} yr^{-1} [*Aber et al.,* 1993]. If atmospheric inputs of N are distributed uniformly within these pools, deposition may have only small effects on the ecosystem, although long-term cumulative effects might be important [*Wedin and Tilman,* 1996]. However, atmospheric inputs of N are roughly half the green foliar N content (100-150 mmol m^{-2}) and nearly equal to the N deposited in litter (60-70 mmol m^{-2} yr^{-1}). Foliar absorption of N could lead to more significant effects by atmospheric N, and atmospheric input of N, if it is efficiently converted to woody biomass, with C:N ratio = 200, could support carbon storage rate of 1.6 t C ha^{-1} yr^{-1} [*Schindler and Bayley,* 1993], comparable to the net carbon accumulation observed at Harvard Forest for the period 1991-1995 (1.4-1.8 ton-C ha^{-1} yr^{-1}) [*Goulden et al.,* 1996b].

4.2 Meteorological and Seasonal Factors

Nitrogen deposition measured at Harvard Forest depends on wind patterns that control transport from source regions, frequency and amount of precipitation, oxidizing capacity of the atmosphere, and other factors. Mean NO_y concentrations and eddy fluxes were higher for periods with southwesterly winds, the direction associated with transport from east coast urban areas, and with trajectories originating in the Great Lakes/Ohio Valley region [*Moody et al.,* 1998] (see Table 1). Periods with frequent wet weather or above average rainfall amounts are also associated with enhanced N deposition. A least-squares fit to a linear model of the data that predicts N deposition by season, the percentage of winds from the SW sector, and the frequency of rainfall gave a multiple R^2 of 0.65 (see Table 2a). The regression model identifies a significant ($p < 0.01$) seasonal component with an amplitude of 40 μmol m^{-2} d^{-1} (Table 2b) accounting for 38% of the variance in the data. The variations in N deposition due to differences in frequency of SW wind and precipitation account for an additional 17% and 11% of variance, respectively. Each of the estimated effects for the observed range of SW wind and precipitation frequency is about 30 μmol m^{-2} d^{-1}. We attribute the influence of wind direction to advection from source regions and

the influence of precipitation frequency on scavenging processes. We argue below that the seasonal dependence of NO_y deposition is due to differences in chemical processing.

4.3 Influence of Rates for Oxidation of NO_2 on NO_y Deposition Flux

4.3.1. Estimated HNO_3 production rates. As M96 noted, direct deposition of NO_2 is a small contribution to the dry deposition of NO_y; HNO_3 and organic nitrates (see below) account for NO_y dry deposition. Aerosol nitrate and HNO_3 are the sources of nitrate in precipitation.. In this section we evaluate the seasonal pattern of production rates for depositing species, HNO_3 and organic nitrates that can be derived from the observed concentrations at Harvard Forest, and compare it with the observed deposition rates. We will consider two inorganic pathways for production of HNO_3: homogeneous oxidation of NO_x ,

$$NO_2 + OH \xrightarrow{k_1} HNO_3, \quad (1)$$

and heterogeneous oxidation, via reactions (2)-(4), culminating in hydrolysis of N_2O_5 on aerosol surfaces. Photolysis, reaction (5), terminates this pathway.

$$NO_2 + O_3 \xrightarrow{k_2} NO_3 \quad (2)$$

$$NO_3 + NO_2 \xrightarrow{k_3} N_2O_5 \quad (3)$$

$$N_2O_5 + H_2O \xrightarrow[\text{aerosol}]{k_4} 2\ HNO_3 \quad (4)$$

$$NO_3 + h\nu \xrightarrow[O_2]{k_5} NO_2 + O_3. \quad (5)$$

We also consider one organic pathway based on formation of hydroxyalkyl nitrates from biogenic hydrocarbons. Oxidation of alkenes by OH generates peroxy radicals that react with NO to form hydroxyalkyl nitrates. The reported yield of hydroxyalkyl nitrates from isoprene reaction is 12% [*Paulson and Seinfeld,* 1992*; Tuazon and Atkinson*, 1990], though it could be less than 5% (*Chen et al.*, submitted to *Journal of Geophysical Research*, 1997). A yield of 17% has been observed for α-pinene [*Noziere et al.,* 1997]. Shorter (2-4 carbon) hydroxyalkyl nitrates have significant Henry's Law constants [*Kames and Schurath,* 1992*; Roberts,* 1990; *Shepson et al.,* 1996] and will dissolve in precipitation or on aerosol. The unsaturated hydroxyalkyl nitrates from isoprene may have similar solubility and, in addition, react with OH [*Shepson et al.,* 1996]. Expected products include dinitrates, acid nitrates, and acetyl nitrate, which readily hydrolyzes [*Trainer et al.,* 1991]. Aerosol nitrate has been observed in smog-chamber reactions of biogenic hydrocarbons [*Hoffmann et al.,* 1997]. Although the detailed chemistry of hydroxyalkyl nitrates has not been worked out, atmospheric models that include them assume they have a deposition velocity and rainfall scavenging efficiency equal to that of HNO_3 [*Horowitz et al.,* 1998*; Liang et al.,* 1998; *Trainer et al.,* 1991]. Production of hydroxyalky nitrates is examined here in order to evaluate this assumption.

We compute the mean and variance of potential HNO_3 production rates in the regional boundary layer surrounding Harvard Forest, using distributions of precursor concentrations for each month defined by means and logarithmic standard deviations of midday data (Table 3). We use

surface measurements during the middle of the day, when vertical mixing is most intense, as the most representative of concentrations throughout the mixed layer. We exclude the high and low extremes (data outside the 12.5 and 87.5 percentiles) that occur in conditions that may not be regionally representative. Temperatures in the mixed layer are adjusted from the surface observations by a 6 ∫C km^{-1} lapse rate. Regionally representative mixed-layer depths are taken from *Holzworth* [1967] to account for seasonal variation in mixing heights. Concentrations and temperature-adjusted rate constants [*DeMore et al.,* 1997] are applied to equations for the rate-limiting reaction in each pathway to yield a set of rates for HNO_3 production.

The homogeneous production of HNO_3 on a 24-hour average basis is given by $k_1 \times [\overline{OH}]$, where $[\overline{OH}]$ is the 24-hour average OH concentration from a three-dimensional chemical tracer model [*Wang et al.,* 1998] that includes detailed NO_x and hydrocarbon chemistry. The predicted OH seasonal cycle has an amplitude consistent with seasonal variations in hydrocarbon concentrations at Harvard Forest [*Goldstein et al.,* 1995]. The resulting production rates depend on seasonal variation in ambient NO_2 and OH concentrations.

We assume that heterogeneous formation of HNO_3 is limited by reaction (2) forming NO_3. For typical particle concentrations in the continental boundary layer and a sticking coefficient, $\gamma = 0.1$ [*DeMore et al.,* 1997], the lifetime of N_2O_5 is shorter than the duration of night. *Dentener and Crutzen* [1993] computed the annual zonal mean lifetime for N_2O_5 as <1 hour in northern midlatitudes below 850 mbar, due primarily to SO_4^{2-} aerosol from anthropogenic sources. The reaction probability for NO_3 with aerosol surfaces in the continental boundary layer is 2 orders of magnitude less than that of N_2O_5 [*Rudich et al.,* 1996]. The rate for heterogeneous formation of HNO_3 from hydrolysis of N_2O_5 is given by $2 \times \int_{t_1}^{t_2} k_2 [O_3][NO_2]dt$. Because NO is fully oxidized to NO_2 at night, we initialize nighttime mixed-layer NO_2 concentrations with midday NO_x ($NO + NO_2$) and allow NO_2 to decay exponentially over time ($NO_2 = NO_x\,(0)\, \exp(-k_2 O_3 t)$). Fresh emissions only replenish NO_x in the shallow nocturnal boundary layer. The rate expression is integrated over the length of night to obtain the production rate for HNO_3. Concentrations of NO_x and O_3 are negatively correlated, particularly in winter ($r = -0.53$), but comparison of calculations using actual data and the random distributions for selected periods did not show any evidence of significant bias. The calculations presented here are intended to evaluate seasonal trends in the regional balance between deposition and HNO_3 production as defined by observed concentrations.

We compute rates for hydroxyalkyl nitrate formation based on the isoprene emissions at Harvard Forest [Goldstein et al., Seasonal course of isoprene emissions from a midlatitude deciduous forest, submitted to *Journal of Geophysical Research,* 1997], a monoterpene:isoprene ratio of 0.25 [*Guenther et al.,* 1995], and hydroxyalkyl nitrate yields of 4.4% and 17% for isoprene and monoterpene, respectively. We make no distinction between direct dry deposition of the hydroxyalkyl nitrates, precipitation scavenging, conversion to HNO_3, or condensation on aerosol surfaces; all processes result in transfer of reactive N from the atmosphere to the surface.

Computed rates for homogeneous production of HNO_3 at Harvard Forest show a seasonal cycle with a winter minimum, a flattened maximum from May through October, and a slight dip in July (Figure 10). The seasonal cycle is driven by seasonality in OH concentrations, but its amplitude is diminished by the offsetting effect of a winter maximum and summer minimum in NO_2 (M96). Rates for heterogeneous processes achieve their maxima in the spring and fall at the crossover points for opposing trends in NO_x and O_3 concentrations (Figure 10, middle). Concentrations of NO_x are at their peak in winter (M96), but lower O_3 concentrations and colder

temperatures reduce rates for formation of NO_3. Note that the variability for estimated heterogeneous HNO_3 production is greatest in the spring and fall months as well. Rapid NO_x oxidation should occur during pollution episodes with elevated NO_x and O_3, with much slower rates at other times. Production of hydroxyalkyl nitrates begins in June and reaches a maximum in July and August that is comparable to the inorganic HNO_3 production terms (Figure 10, bottom panel).

Computed rates for heterogeneous and homogeneous HNO_3 production roughly balance the mean deposition rate observed at Harvard Forest during winter and fall (Figure 11). In summer, however, inorganic production of HNO_3 does not balance the observed deposition. Concentration profiles at Harvard Forest are not consistent with NO_2 having a large deposition velocity (M96), but even a deposition velocity of 1 cm s^{-1} would not account for the imbalance because NO_2 concentrations are too small.. The apparent deficit in NO_x oxidation during the growing season points to a mechanism linked to vegetation. The seasonality of hydroxyalkyl nitrate formation roughly matches the apparent excess in N deposition. However, its absolute magnitude is less certain, because mean hydrocarbon fluxes for the region must be estimated, and the complete chemical mechanism for this series of reactions has not been determined. Terpene emissions may be relatively more important in the spring and fall when conifers are active but oaks are dormant. The magnitude of hydroxyalkyl nitrate-mediated NO_x oxidation that we estimate for the northeastern United States. is in agreement with model predictions that this process accounts for 25% of the NO_y deposition in North America during summer [*Liang et al.*,1997].

At the remote site, near Schefferville, computed local production of HNO_3 is 2.2 μmol m^{-2} d^{-1} in summer, only about 10% of the observed average deposition, 20 μmol m^{-2} d^{-1}, but comparable to the minimum observed deposition (Figure 8). We noted previously that a few episodes accounted for a large proportion of the total N deposition at Schefferville, such as the rain event on July 30 and the elevated dry deposition on July 1-5 (Figure 8). *Bakwin et al*. [1994] attributed these events to advection of pollutants associated with passage of high-pressure systems that import depositing species of NO_y from urban-industrial centers.

4.3.2. Characteristic times for NO_y oxidation and deposition. We can directly estimate the time constants, τ, for NO_x oxidation by setting the concentrations of O_3 and OH to their monthly mean values (Table 3) and evaluating the relevant rate expression, for example, $\tau = (k_1[OH])^{-1}$ for reaction (1). The characteristic time for deposition of NO_x oxidation products is calculated as column mass divided by total (wet plus dry) flux, analogous to the wet-deposition lifetimes reported by *Doddridge et al*. [1992] for NO_y over Virginia. We estimated column mass by integrating the midday surface mixing ratio over the boundary layer depth ($\int_0^H X\,\rho(z)dz$) where X is the mixing ratio and ρ is the air density. The characteristic time for hydroxyalkyl nitrate formation is determined from the NO_x column mass divided by the scaled isoprene flux.

The characteristic times for both NO_2 oxidation by OH and hydroxyalkyl nitrate formation are <0.5 day in summer and increase at least ten fold in winter (Figure 12, top). However, the characteristic time for heterogeneous reaction is more uniform;, thus the overall chemical lifetime increases from a minimum of 0.3 day in summer to only 1.5 days in winter as the limiting oxidant shifts from OH to O_3 (Figure 12). The characteristic time for removal of NO_x oxidation products (NO_y-NO_x), τ_{dep}, is around 1 day for most of the year and decreases to 0.4 day in winter when NO_x:NO_y is highest (Figure 12). The characteristic time expressed in terms of total NO_y, which is the effective time constant for oxidation and deposition acting in series [*Parrish et al.*, 1991], ranges from 1 day in mid summer to more than 2 days in winter months. The shorter

characteristic time for deposition of oxidation products in winter is consistent with shallower mixed layer and also with reduced contribution from non-depositing species, such as alkyl nitrates, to the mix of NO_x oxidation products. These values are in agreement with the lifetimes that *Parrish et al.* [1991] find consistent with observed NO_y:CO ratios in summer at Niwot Ridge.

At Schefferville, lower OH and O_3 concentrations account for chemical lifetimes of 1.0 day and 2.1 days, respectively, for oxidation by OH and O_3. The characteristic time for deposition of NO_y - NO_x at Schefferville, 0.76 day, is slightly less than that at Harvard Forest.

Figure 12 shows that removal of NO_x oxidation products (NO_y - NO_x) takes slightly longer than their production for most of the year. Hence, within the region surrounding Harvard Forest, NO_x oxidation products tend to build up in relation to the total reactive N concentration. Relatively long lifetimes for deposition are consistent with the observation that some HNO_3 remains when an air parcel reaches a remote area such as Schefferville, where local oxidation of ambient NO_x accounts for only 10% of NO_y deposition. Because NO_x oxidation is so rapid, the NO_x observed at Schefferville is likely to arise from decomposition of PAN or other long-lived species transported there, rather than as NO_x [*Fan et al.*, 1994]. Thus the fraction of NO_x converted to stable organics is critical for supplying reactive N to the remote troposphere. Our results imply that, at Schefferville, NO_x is provided by decomposition of reservoir species such as PAN [*Singh and Hanst*, 1981] and that PAN also supports background levels of NO_y. Episodic transport of HNO_3 and other nonradical species accounts for high levels of NO_y and pulses of N deposition.

Fluxes of NO_y are a factor of 6 smaller ($\approx e^{-2}$) at Schefferville than at Harvard Forest, somewhat less than the decline in concentration. Assuming comparable emission rates in source areas upwind, this finding suggests 2-3 days transport time to Schefferville.

4.3.3. NO_y budget integration. From the differential equations for rates of NO_x oxidation and deposition ($dNO_x = -k_c NO_x dt$, and $dHNO_3 = (k_c NO_x - k_d HNO_3)dt$, respectively) we can derive a simple expression to predict the concentration of HNO_3 in the boundary layer downwind of a major source region,

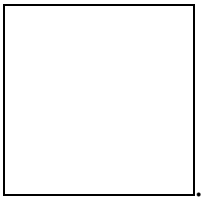

(6)

Here $HNO_3(t)$ is the concentration of HNO_3 (and other rapidly deposited compounds) at time after emission, t, $NO_x(0)$ is the initial concentration of NO_x at the emission source, and k_c and k_d are effective first-order rate constants (derived from photochemical calculations and from observations) for photochemical production and deposition, respectively. Note that k_c reflects heterogeneous, homogeneous, and organic pathways for conversion of NO_x to HNO_3 (or other rapidly depositing species) and k_d accounts for total (wet plus dry) deposition. We include a dilution factor, D, to account for mixing of the polluted air parcel with cleaner background air (D cancels out of the analysis of ratios of species).

This ultra-simple model allows us to assess the fraction of NO_x deposited in the region and the extent of the receptor area, using fluxes and concentrations of NO_y observed at a single station. The model illustrates the consequences of seasonal trends in reaction and deposition rates and

provides a first estimate for the fraction exported. We use mean concentrations and rates for chemical reactions and deposition, and we treat individual parcels independently. In reality, oxidant concentrations, and hence reaction rates, depend somewhat on concentrations of NO_x [*Logan et al.,* 1981], but the largest variations in the rates for deposition reflect seasonal changes in solar radiation, concentrations of water vapor, and boundary layer characteristics.

The model does not account for formation and recycling of PAN, which may have a long lifetime if it is transported above the boundary layer. The data analysis given above showed that the average reactive-N deposition rate at Harvard Forest closely matches the regional emission rate. Hence it is unlikely that the regional budget is strongly affected by ventilation of PAN from the boundary layer. However, the role of such processes in the supply of NO_x to the global environment is unclear: the fraction escaping is predicted to be small [*Horowitz et al.*, 1998; *Liang et al.*, 1998] and consequently difficult to determine accurately by measurements of deposition.

The key feature of the boundary layer in summer, fall, and spring is that the NO_x oxidation rate constant exceeds the deposition rate constant for the oxidation products; hence oxidation products make an increasing fraction of total NO_y, and the ratio $NO_x/(NO_x+HNO_3)$ decreases with time (Figure 13, top). Observed values of NO_x:NO_y = 0.25 (M96) at noon during summer at Harvard Forest are consistent with transit times of <1 day, or mixtures of older emissions that have been depleted of NO_x with fresh NO_x emitted from sources a few hours upwind. Recycling of PAN may provide an input of NO_x to maintain the NO_x:NO_y ratio at Schefferville near 0.2 (M96) rather than approaching 0 as predicted for transit times of >1 day. During winter the rate constant for deposition of NO_x oxidation products exceeds the rate constant for NO_x oxidation; the $NO_x/(NO_x+HNO_3)$ ratio for long times approaches a constant, ≈0.6, comparable to observed NO_x:NO_y ratios (M96).

The product of $k_d \times f_{HNO_3}$ defines the fraction of initial NO_x deposited in unit time at travel time t downwind, where f_{HNO_3} is the fraction of odd nitrogen present as HNO_3 relative to the initial NO_x ($f_{HNO_3} \equiv HNO_3(t)/\{NO_x(0)/D\} = k_c/(k_d - k_c)(e^{-k_c t} - e^{-k_d t})$). The value of f_{HNO_3} is zero at the emission source (t=0), increases downwind to a maximum, and then gradually declines to 0 as NO_x is oxidized and deposited (Figure 13, middle). Note that because the parcel is dispersing with time, concentrations and deposition per unit area typically decline with increasing distance from the source. For summer conditions the peak in f_{HNO_3} occurs at ages of <1 day, while for winter conditions with slower chemistry the peak is delayed and broadened such that f_{HNO_3} in winter exceeds the summer values for parcel ages of >2 days.

Integration of $k_d \times f_{HNO_3}$ over time gives the cumulative fraction of NO_x deposited (Figure 13, bottom): 45% for t = 1 day in summer, 27% in winter. The time required to remove 95% of NO_x is 3.5 days in summer and 5 days in winter. This analysis indicates that transport and dispersion of NO_x in the boundary layer cannot account for most of the atmospheric N in the remote troposphere, because oxidation of NO_x and deposition of HNO_3 are efficient. Observations of NO_y accumulation in the wintertime troposphere at high latitudes [e.g. *Bottenheim et al.*, 1993*; Dickerson et al.,* 1985; *Muthuramu et al.,* 1994] could be accounted for by formation of stable species such as alkyl nitrates and PANs that have longer lifetimes but are not included in our analysis.

5. Conclusions

In this paper we have used 7 years of measurements at Harvard Forest, 1-2 days downwind of a major source region, to compute the rates for NO_x oxidation and HNO_3 deposition, to determine the reactive-N budget at the site, and to estimate the fraction of N removed in the region

near the source. We found annual average input of 47 mmol m^{-2} yr^{-1}, with about twice as much wet as dry deposition. Variations in partitioning between wet and dry deposition tended to offset each other because HNO_3, the main depositing species, is removed efficiently by both processes. Nitrogen deposition at Schefferville was a factor of ~6 less (20 μmol m^{-2} d^{-1} versus. 130 μmol m^{-2} d^{-1}) during the summer than the mean summertime rate at Harvard Forest, consistent with a transport time of 2-3 days from emission sources.

Analysis of the regional balance between production and deposition allows us to infer reaction and deposition lifetimes for NO_x in the boundary layer. The lifetimes for oxidation of NO_x ranged from 0.24 day in summer, due to the combined effect of homogeneous, heterogeneous, and organic pathways, to 1.4 days in winter, due to heterogeneous processes alone. The lifetimes for deposition of HNO_3 were 1 and 0.6 day in summer and winter, respectively.

Our analysis shows that deposition of reactive N is regulated by the rate of oxidation of NO_x by reactions with HO_x radicals, by heterogeneous reactions of N_2O_5, and by organic pathways. Contributions from these three processes are comparable during summer; heterogeneous and organic pathways for NO_x oxidation are more important than we expected them to be. The presence of forests downwind of source regions enhances rates for nitrogen deposition and increases the fraction of NO_x retained in the region, because forests are efficient, aerodynamically rough receptors and because biogenic hydrocarbons emitted by vegetation accelerate the rate of oxidation of NO_x.

The NO_x emitted from eastern North America is efficiently retained in the region during summer. Export about doubles from summer to winter, but heterogeneous production of HNO_3 is efficient, and ventilation of the boundary layer is relatively slow; hence most of the emitted NO_x is probably deposited further downwind. Thus remote sites such as Schefferville, 2-3 days' transport from the emission sources, could receive most of their annual reactive-N input during winter when it accumulates in the snowpack and becomes available during spring melt. Only a small fraction of N escapes to the global environment in either season.

Acknowledgments. This work was supported by grants from the National Aeronautics and Space Administration (NAG1-55, NAGW-3082), from the National Science Foundation (BSR-89-19300), from the U.S. Department of Energy to Harvard University (Northeast Regional Center of the National Institute for Global Environmental Change, DOE Cooperative Agreement DE-FC03-90ER61010), by Harvard University (Harvard Forest and Division of Applied Sciences), by the Electric Power Research Institute, and by the Alexander Host Foundation (fellowship to PSB). The Harvard Forest tower is a component of the Long-Term Ecological Research (LTER) site at Harvard Forest. We thank the staffs of the McGill Subarctic Research Station and the NASA Langley Research Center for logistical support at Schefferville during the ABLE 3B study. We thank the Harvard Forest woods crew for their assistance. We particularly thank B. Daube, A. Hirsch, S. Roy, D. Sutton, F. Gimmelfarb, and C. Nielsen for their contributions to this project. We thank D. Jacob, L. Horowitz, and Y. Wang for helpful discussions. The complete Harvard Forest data set is available from http://www-as.harvard.edu.

References

Aber, J. D., A. Magill, R. Boone, J. M. Melillo, P. Steudler, and R Bowden, Plant and soil responses to chronic nitrogen additions at the Harvard Forest, Massachusetts, *Ecol. Appl., 3*, 156-166, 1993.

Bakwin, P. S., et al., Reactive nitrogen oxides and ozone above a taiga woodland, *J. Geophys. Res., 99*, 1927-1936, 1994.

Bottenheim, J.W., L. A. Barrie, and E. Atlas, The partitioning of nitrogen oxides in the lower Arctic troposphere during spring 1988, *J. Atmos. Chem., 17*, 15,.1993.

Chambers, J. M., and T. J. Hastie (Eds.), *Statistical Models in S*, 608, pp. Wadsworth, Belmont, Calif., . 1992.

Davidson, E. A., Fluxes of nitrous oxide and nitric oxide from terrestrial ecosystems, in *Microbial Production and Consumption of Greenhouse Gases: Methane, Nitrogen Oxides, and Halomethanes*, edited by. W. B. Whitman, pp. 219-235, Am. Soc. for Microbiol., Washington, D. C., 1991.

DeMore, W. B., S. P. Sander, D. M. Golden, R. F. Hampson, M. .J. Kurylo, C. J. Howard, A. R. Ravishankara, C. E. Kolb, and M. J. Molina, Chemical kinetics and photochemical data for use in stratospheric modeling, evaluation number 12, *JPL Pub*., *97*-4, 1997.

Dentener, F. J., and P. J. Crutzen, Reaction of N_2O_5 on tropospheric aerosols: Impact on the global distributions of NO_x, O_3, and OH, *J. Geophys. Res.*, *98*, 7149-7163, 1993.

Dickerson, R. R., Reactive nitrogen compounds in the arctic, *J. Geophys. Res.*, *90*, 10,739-10,743, 1985.

Doddridge, B.G., R. R. Dickerson, R. G. Wardell, K. L. Civerolo, and L. J. Nunnermacker, Trace gas concentrations and meteorology in rural Virginia, 2,. Reactive nitrogen compounds, *J. Geophys. Res. 97*, 20,631-20,646, 1992.

Environmental Protection Agency (EPA), The 1985 NAPAP emission inventory (version 2): Development of the annual data and modeler's tapes, *Rep. EPA-600/7-89-012a*, Research Triangle Park, N. C., 1989.

Fan, S.-M., D. J. Jacob, D. L. Mauzerall, J. D. Bradshaw, S. T. Sandholm, D. R. Blake, H. B. Singh, R. W. Talbot, G. L. Gregory, and G. W. Sachse, Origin of tropospheric NO_x over subarctic eastern Canada in summer, *J. Geophys. Res.*, *99*, 16,867-16,877, 1994.

Fitzjarrald, D. R., and K. E. Moore, Growing season boundary layer climate and surface exchanges in the northern lichen woodland, *J. Geophys. Res*., *99*, 1899-1917, 1994.

Galloway, J. N., W. H. Schlesinger, H. Levy II, A. Michaels, and J. N. Schoor, Nitrogen fixation: Anthropogenic enhancement-environmental response, *Global Biogeochem. Cycles, 9*, 235-252, 1995.

Goldstein, A. H., C. M. Spivakovsky, and S. C. Wofsy, Seasonal variations of nonmethane hydrocarbons in rural New England: Constraints on OH concentrations in northern midlatitudes, *J. Geophys. Res., 100*, 21,023-21,033, 1995.

Goulden, M. L., J.W. Munger, S.-M. Fan, B. C. Daube, and S. C. Wofsy, Measurements of carbon sequestration by long-term eddy covariance: Methods and a critical evaluation of accuracy, *Global Change Biol., 2*, 169-182, 1996a.

Goulden, M. L., J .W. Munger, S.-M. Fan, B. C. Daube, and S. C. Wofsy, Exchange of carbon dioxide by a deciduous forest: Response to interannual climate variability, *Science, 271*, 1576-1578, 1996b.

Guenther, A., et al., A global model of natural volatile organic carbon emissions, *J. Geophys. Res., 100*, 8873-8892, 1995.

Hanson, P. J,. and S. E. Lindberg, Dry deposition of reactive nitrogen compounds: A review of leaf, canopy and non-foliar measurements, *Atmos. Environ*., *Part A, 25*, 1615-1634, 1991.

Hoffmann, T., J. R. Odum, E. W. Bowman, D. H. Collins, D. Klockow, R. C. Flagan, and J. R. Seinfeld, Formation of organic aerosols from the oxidation of biogenic hydrocarbons, *J. Atmos. Chem.*, *26*, 189-222, 1997.

Holland, E. A., et al., Variations in the predicted spatial distribution of atmospheric nitrogen deposition and their impact on carbon uptake by terrestrial ecosystems, *J. Geophys. Res., 102*, 15,849-15,866, 1997.

Holzworth, G. C., Mixing depths, wind speeds and air pollution potential for selected locations in the United States, *J. Appl. Meteorol*., *6*, 1039-1044, 1967.

Horowitz, L.W., D. J. Jacob, J. L. Liang, and G. M. Gardner, Export of reactive nitrogen from North America during summertime: Sensitivity to hydrocarbon chemistry, *J. Geophys. Res.*, in press, 1998.

Johnson, D. W. and S. E. Lindberg, *Atmospheric Deposition and Forest Nutrient Cycling*, 707 pp., Springer-Verlag, New York, 1992.

Kames, J., and U. Schurath, Alkyl nitrates and bifunctional nitrates of atmospheric interest: Henry's law constants and their temperature dependencies, *J. Atmos. Chem.*, *15*, 79-95, 1992.

Lefer, B. L., The chemistry and dry deposition of atmospheric nitrogen at a rural site in the northeastern United States, Ph.D. thesis, 119 pp., University of New Hampshire, December, 1997.

Liang, J., D. J. Jacob, L. W. Horowitz, G. J. Gardner, and J. W. Munger, Seasonal budgets of reactive nitrogen species and ozone over the United States, and export fluxes to the global atmosphere, *J. Geophys. Res.* in press, 1998.

Liu, S. C., M. Trainer, F. C. Fehsenfeld, D. D. Parrish, E. J. Williams, D. W. Fahey, G. Hubler, and P. C. Murphy, Ozone production in the rural troposphere and the implications for regional and global ozone distributions, *J. Geophys. Res. 92*, 4191-4207, 1987.

Logan, J. A., M. J. Prather, S. C. Wofsy, and M. B. McElroy, Tropospheric chemistry: A global perspective, *J. Geophys. Res., 86*, 7210-7254, 1981.

Logan, J. A., Nitrogen oxides in the troposphere: Global and regional budgets, *J. Geophys. Res., 88*, 10,785-10,807, 1983.

Meyers, T. P., B. B. Hicks, R. P. Hosker Jr., J. D. Womack, and L. C. Satterfield, Dry deposition inferential measurement techniques, II, Seasonal and annual deposition rates of sulfur and nitrate, *Atmos. Environ, Part A, 25*, 2361-2370, 1991.

Moody, J. L., J. W. Munger, A. H. Goldstein, D. J. Jacob, S. C. Wofsy, Harvard Forest regional-scale airmass composition by PATH (Patterns in atmospheric transport history), *J. Geophys. Res.*, in press, 1998.

Munger, J. W., S. C. Wofsy, P. S. Bakwin, S.-M. Fan, M. L. Goulden, B. C. Daube, A. H. Goldstein, K. E. Moore, and D. R. Fitzjarrald, Atmospheric deposition of reactive nitrogen oxides and ozone in a temperate deciduous forest and a subarctic woodland, 1, Measurements and mechanisms, *J. Geophys. Res., 101*, 12,639-12,657, 1996.

Muthuramu, K., P. B. Shepson, J. W. Bottenheim, B. T. Jobson, H. Niki, and K. G. Anlauf, Relationships between organic nitrates and surface ozone destruction during Polar Sunrise Experiment 1992, *J. Geophys. Res., 99*, 25,369- 25,378, 1994.

Nozière, B., I. Barnes, and K. Becker, Gas-phase oxidation of α-pinene initiated by OH radicals in the presence of NO_x: Product and mechanistic study; Identification and thermal stability of a terpenoid derived PAN analogue, paper presented at Workshop on biogenic hydrocarbons in the atmospheric boundary layer, Charlottesville, Aug. 24 to 27, 1997.

Ollinger, S. V., J. D. Aber, G. M. Lovett, S. E. Millham, R. G. Lathrop, and J. M. Ellis, A spatial model of atmospheric deposition for the northeastern U. S., *Ecol. Appl., 3*, 459-472, 1993.

Parrish, D. D., M. Trainer, M. P. Buhr, B. A. Watkins, and F. C. Fehsenfeld, Carbon monoxide concentrations and their relation to concentrations of total reactive oxidized nitrogen at two rural U.S. sites, *J. Geophys. Res., 96*, 9309-9320, 1991.

Paulson, S. E., and J. H. Seinfeld, Development and evaluation of a photooxidation mechanism for isoprene, *J. Geophys. Res., 97*, 20,703-20,715, 1992.

Prather, M., R. Derwent, D. Ehhalt, P. Fraser, E. Sanhueza, and X. Zhou, Other trace gases and atmospheric chemistry, in *Climate Change 1994*: *Radiative Forcing of Climate Change and an Evaluation of the IPCCIS92 Emission Scenarios*, chap. 2, Cambridge Univ. Press, Cambridge, 1995.

Roberts, J. M., The atmospheric chemistry of organic nitrates, *Atmos. Environ. 24A*, 243-287, 1990.

Rudich, Y., R. K. Talukdar, A. R. Ravishankara, and R. W. Fox, Reactive uptake of NO_3 on pure water and ionic solutions, *J. Geophys. Res., 101*, 21,023-21,231, 1996.

Schindler, D. W., and S. E. Bayley, The biosphere as an increasing sink for atmospheric carbon: Estimates from increased nitrogen deposition, *Global Biogeochem. Cycles, 7*, 717-733, 1993.

Shepson, P. B., E. Mackay, and K. Muthuramu, Henry's Law constants and removal processes for several atmospheric β-hydroxy alkyl nitrates, *Environ. Sci. Technol., 30*, 3618-3623, 1996.

Singh, H. B., and P. L. Hanst, Peroxyacetyl nitrate (PAN) in the unpolluted atmosphere: An important reservoir for nitrogen oxides, *Geophys. Res. Lett., 8*, 941-944, 1981.

Tjepkema, J. D., R. J. Cartica, and H. F. Hemond, Atmospheric concentration of ammonia in Massachusetts and deposition on vegetation, *Nature, 294*, 445-446, 1981.

Trainer, M., et al., Observations and modeling of the reactive nitrogen photochemistry at a rural site, *J. Geophys. Res*., *96,* 3045-3063, 1991.

Tuazon, E. C., and R. Atkinson, A product study of the gas-phase reaction of isoprene with the OH radical and the presence of NO_x, *Int. J. Chem. Kinet.*, *22*, 1221-1236, 1990.

Wang, Y., J. A. Logan, and D. J. Jacob, Global simulation of tropospheric O_3-NO_x-hydrocarbon chemistry, 2., Model evaluation and global ozone budget, *J Geophys. Res.*, in press, 1998.

Wedin, D. A., and D. Tilman, Influence of nitrogen loading and species composition on the carbon balance of grasslands, *Science, 274*, 1720-1723, 1996.

P. S. Bakwin, Climate Monitoring and Diagnostics Laboratory, National Oceanic and Atmospheric Administration, 325 Broadway, Boulder, CO 80303.

A. S. Colman, Department of Geology and Geophysics, Yale University, New Haven, CT 06511.

S.-M. Fan, Atmospheric & Oceanic Sciences Program, Princeton University, Princeton, NJ 08544.

A. H. Goldstein, Department of Environmental Science, Policy, and Management, University of California, Berkeley, Berkeley, CA. 94720.

M. L. Goulden, Department of Earth System Science, University of California, Irvine, Irvine, CA. 92697-3100

J. W. Munger and S. C. Wofsy, Department of Earth and Planetary Sciences, Harvard University, 20 Oxford Street, Cambridge, MA 02138. (e-mail: jwm@io.harvard.edu; scw@io.harvard.edu)

(Received April 22, 1997; revised January 5, 1998;
accepted January 9, 1998.)

[1] Now at Atmospheric & Oceanic Sciences Program, Princeton University, Princeton, New Jersey.

[2] Now at Climate Monitoring and Diagnostics Laboratory, National Oceanic and Atmospheric Administration, Boulder, Colorado.

[3] Now at Department of Earth System Science, University of California, Irvine, Irvine.

[4] Now at Department of Environmental Science, Policy, and Management, University of California, Berkeley.

[5] Now at Department of Geology and Geophysics, Yale University, New Haven Connecticut.

Paper number 98JD00168.
0148-0227/98/98JD-00168$09.00

Table 1. Quarterly Statistics for N deposition and Meteorological Conditions at Harvard Forest

Season[a]	Year	Total N Deposition, μmol m^{-2} d^{-1}	Frequency of Surface Winds by Sector			Frequency of Rain[b], %	Rainfall amount[b], mm
			Northwest (270°- 45°), %	East (45°-180°), %	Southwest (180°-270°), %		
Spring	1990	205	46.6	12.8	40.2	50.0	337.9
Summer	1990	139	40.3	21.9	37.2	39.1	271.3
Fall	1990	132	44.7	16.8	38.0	30.8	263.8
Winter	1991	103	52.9	15.3	31.4	40.1	311.2
Spring	1991	105	57.1	17.0	25.7	35.8	309.6
Summer	1991	168	51.1	17.5	31.0	33.8	420.0
Fall	1991	135	48.3	16.3	35.2	35.2	408.4
Winter	1992	81	55.6	16.0	28.1	39.4	210.6
Spring	1992	146	47.2	26.9	25.9	34.8	293.9
Summer	1992	161	48.0	16.6	35.1	49.8	390.5
Fall	1992	135	46.5	19.1	34.2	46.2	272.1
Winter	1993	110	48.8	24.4	26.5	47.6	222.8
Spring	1993	128	45.1	26.7	28.0	53.4	282.1
Summer	1993	197	51.5	15.3	32.9	53.3	356.0
Fall	1993	168	34.5	20.1	44.8	60.4	357.6
Winter	1994	116	49.2	21.0	29.5	47.6	357.6
Spring	1994	151	44.2	19.2	36.1	53.3	362.1
Summer	1994	169	32.6	18.5	48.4	47.9	474.5
Fall	1994	59	54.8	19.0	25.6	28.0	NA
Winter	1995	103	52.4	20.5	26.7	28.9	370.0
Spring	1995	103	49.0	23.9	26.9	33.7	262.6
Summer	1995	107	38.3	19.5	41.3	29.4	200.1[c]
Fall	1995	108	42.3	24.0	33.5	34.1	472.4
Winter	1996	58	52.1	21.5	26.1	38.6	252.7
Spring	1996	159	46.2	18.9	34.8	31.5	322.9
Summer	1996	151	40.2	18.0	41.5	26.7	NA
Fall	1996	103	50.9	21.6	27.1	NA	NA

[a] We define the seasons as follows; winter is December through February, spring is March through May, summer is June through August, and fall is September through November.
[b] NA signifies periods with gaps in the precipitation data record.
[c] Invalid rain gauge data for June-August 1995 have been replaced by data from an adjacent site about 10 km north.

Table 2a. Regression Results for the Linear Model fit of N Deposition Predicted by Seasonality and Frequency of Precipitation

	Analysis of Variance Results			
Predictor	Degrees of Freedom	Sum of Squares	Mean Square	Pr(F)[a]
Season	3	12,930.	4,311.0	0.002
SW winds	1	5,930.	5,930.0	0.006
Frequency. of precipitation	1	3,597.	3,597.0	0.026
Residual	19	11,700.	615.7	

	Regression coefficients[b]	
Factor	Coefficient	Standard Error.
Intercept (a_0),μmol m^{-2} d^{-1}	129	5.0
season 1, μmol m^{-2} d^{-1}	-8	9.2
season 2, μmol m^{-2} d^{-1}	16	8.6
season 3, μmol m^{-2} d^{-1}	16	10.0
SW winds, μmol m^{-2} d^{-1} $\%^{-1}$	2.0	1.1
Frequency of Precipitation, μmol m^{-2} d^{-1} $\%^{-1}$	1.5	0.6

$N_{DEP} = a_0 + \Sigma a_1^j s_j + a_2 SW + a_3 FP + \varepsilon$.

[a] Probability based on F distribution for the given degrees of freedom that the observed trends are random.

[b] Regression coefficients are computed for the intercept (annual mean), the seasonal factors, which are transformed to obtain ordered orthogonal factors [*Chambers and Hastie*, 1992], and the response to changes in percentage of time with SW wind and to changes in frequency of rain.

Table 2b. Mean Annual Cycle for N Deposition at Harvard Forest Derived From Seasonal Factors.

Season	Deviation from annual mean[a], μmol m^{-2} d^{-1}
Spring	16
Summer	16
Fall	-8
Winter	-24

[a] The value for the fourth season is set by the requirement that the seasonal cycle sum to zero

.

Table 3. Input Parameters for Estimation of Reaction Rates and Characteristic Times of NO_y Reaction and Deposition.

		NO_y		NO_x		NO_2		O_3				
Month	NO_y Deposit, μmol m^{-2} d^{-1}	Geometric. Mean, ppt	lsd[a]	Geometric Mean, ppt	lsd[a]	Geometric Mean, ppt	lsd[a]	Arithmetic Mean, ppb	s.d., ppb	OH[b], 10^6 molecules. cm^{-3}	T, ∫C	Mixing Height[c], m
Jan.	94.8	5254	0.51	3279	0.55	2688	0.58	27	5.24	0.1	-5	730
Feb.	91.3	6158	0.4	2796	0.56	2162	0.59	34	4.35	0.19	-4.4	900
March	121.9	5095	0.38	2110	0.5	1657	0.53	41	4.27	0.43	0.9	1200
April	139.4	3898	0.38	1282	0.54	1023	0.57	45	4.31	0.78	5.8	1800
May	159.4	3402	0.33	903	0.39	740	0.41	45	5.28	1.25	11.8	1800
June	128.2	2918	0.32	703	0.22	604	0.23	46	5.82	1.7	17.3	1800
July	183.7	3073	0.35	677	0.24	558	0.27	46	7.86	1.83	19.8	1800
Aug.	169.6	3547	0.33	772	0.34	661	0.35	44	6.18	1.5	19.2	1800
Sept.	131.9	3513	0.39	1138	0.44	920	0.47	35	4.75	0.89	14.3	1600
Oct.	122	5075	0.43	1979	0.52	1666	0.53	32	3.83	0.42	10.2	1500
Nov.	108.8	6737	0.43	3535	0.48	2974	0.5	27	3.44	0.16	3	1000
Dec.	107.8	5658	0.52	3226	0.49	2739	0.5	26	4.04	0.08	-2.1	750

Means and standard deviations for the concentrations are computed from the central 50% of the data for each month
[a] Standard deviation of log-transformed data.
[b] OH concentrations from *Wang et al.* [1998].
[c] Mixed-layer height from *Holzworth,* [1967].

Figure Captions

Figure 1. Location of Harvard Forest, indicated by cross, in relation to NO_x emission densities (NAPAP emission inventory [*EPA*,1989]) in the northeastern United States. Darker colors indicate increasing emission density. The origin points of 8-hour back trajectories [*Moody et al.*, 1998] are indicated by contours showing the number of trajectories (of a total of 1276) originating in a cell.

Figure 2. (top) Distribution of hourly NO_y eddy flux values for observations made between 1000 and 1200 during days in July. Data are plotted against quantiles of a normal distribution. A lognormally distributed data set would plot on a straight line. The dashed line connects the upper and lower quartiles of the data. (bottom) Daily integrated NO_y eddy fluxes for July at Harvard Forest (pluses) and for the ABLE 3B Schefferville site (squares). The dotted line connects the tenth and ninetieth percentile of the Harvard Forest data; the dashed line connects twenty-fifth and seventy-fifth percentile of the Schefferville data.

Figure 3. Mean values computed for 100 random subsamples drawn from the set of all NO_y eddy-flux data for the period 1000-1200 in July and August. The ranges of these means normalized by the overall mean are plotted against the fraction of data used in the subsamples. The dashed lines show the corresponding range of mean values for subsamples drawn from a random lognormal distribution based on the mean and standard deviation of the original data.

Figure 4. (top) Average NO_3^- concentrations in rainwater at Harvard Forest (pluses) and at the Quabbin Reservoir National Atmospheric Deposition site (NADP, 1997) for the period 1982 through June 1996 (solid line); dashed lines are the standard error of the monthly means for the Quabbin data. (bottom) Mean NO_3^- deposition by precipitation at Harvard Forest for the period 1990-1995 (solid line) and at the Quabbin Reservoir NADP site (dashed line). The overall mean for the period 1982-1996 at the Quabbin site is given by open triangles.

Figure 5. Mean NO_y dry-deposition fluxes computed for monthly time intervals. Mean fluxes are computed for 50 random subsamples separately for each hour of the day and then summed to give the mean value of integrated daily NO_y dry-deposition flux during that month. Vertical segments give the standard deviation of the 50 subsample means. The seasons, winter (DJF), spring (MAM), summer(JJA), and fall (SON) are denoted by different symbols as indicated in the legend.

Figure 6. Total (wet plus dry) monthly NO_y deposition at Harvard Forest for the period 1900-1996. Light shading indicates the monthly precipitation input; dark shading is the dry deposition (see Figure 5).

Figure 7. Monthly mean deposition of reactive N at Harvard Forest computed from the 1990-1996 data. Dark shading (upper bar) is the input from dry deposition, light shading (lower bar) is the precipitation input. The thin vertical lines indicate the sampling uncertainty for each monthly estimate determined from the standard deviation of the means of random subsamples of the data. The dashed lines are the overall sampling uncertainty for the total deposition. The dot-dashed line indicates the mean NO_x emission rate within 250 km radius of Harvard Forest given by NAPAP emission inventories [*EPA*, 1989].

Figure 8. Total reactive N deposition at Schefferville during summer 1990. Precipitation inputs are shown as light shading; dry deposition is shown as dark shaded bar. Days with too many missing data are seen as gaps in the dry-deposition time series.

Figure 9. Estimated NH_4-N input from precipitation at Harvard Forest determined from the NH_4^+:SO_4^{2-} ratio at Quabbin Reservoir NADP site (NADP, 1997) and the measured SO_4^{2-} deposition in precipitation at Harvard Forest.

Figure 10. Computed production of HNO_3 by (top) NO_2 + OH and (middle) NO_2 + O_3 reactions for observed concentrations of NO_x, NO_2, O_3, and air temperatures at Harvard Forest and typical values of OH and mixed layer depths in the northeastern United States. For each month, 1000 individual estimates of HNO_3 production were generated by using random values of concentrations picked from data distributions as defined in Table 3. The solid lines with solid circles indicate medians; open circles are the mean values. Long-dashed lines bound the twenty-fifth and seventy-fifth percentiles of the computed values; short-dashed lines are the standard deviations. (bottom) Potential production of hydroxyalkyl nitrates for the observed isoprene emission flux at Harvard Forest (solid line) and the production rate if the isoprene fluxes were a factor of 2 less (dashed line). Corresponding production rates at Schefferville are 1.6 and 0.6 $\mu mol\ m^{-2}\ d^{-1}$ for homogeneous and heterogeneous pathways, respectively.

Figure 11. Total production of HNO_3 by homogeneous (dark shading), heterogeneous (light shading), and hydroxyalkyl nitrate (stippled) pathways in the mixed layer as estimated in Figure 10 versus observed N deposition (solid line) at Harvard Forest. Uncertainty estimates for the production and deposition terms (Figures 7 and 10) are omitted for clarity.

Figure 12. (top) Characteristic (*e*-folding) times for HNO_3 production estimated from modeled OH concentrations, monthly mean observed O_3 concentrations, and isoprene fluxes. (bottom) Deposition lifetimes for NO_y (open circles) and for NO_x oxidation products, $NO_z = NO_y - NO_x$, (solid squares) are determined from the observed deposition flux and column mass. The overall chemical lifetime is the combination of characteristic times for reaction with OH, O_3, and isoprene (dashed line with open triangles). The characteristic times for OH and O_3 oxidation (top) and the overall chemistry and deposition lifetimes (bottom) at Schefferville in summer are indicated by symbols on the right margin (OH, O_3, R, D).

Figure 13. (top) Values of the NO_x ratio, $NO_x/(NO_x+HNO_3)$, (middle) HNO_3 fraction, $f_{HNO_3} = HNO_3(t)/(NO_x(0)/D)$, and (bottom) fraction of NO_x that has been deposited, computed from equation (6) (see text) by using seasonal mean values of reaction and deposition time constants (in days) for chemical reaction (τ_c) and deposition (τ_d) taken from Figure 12.

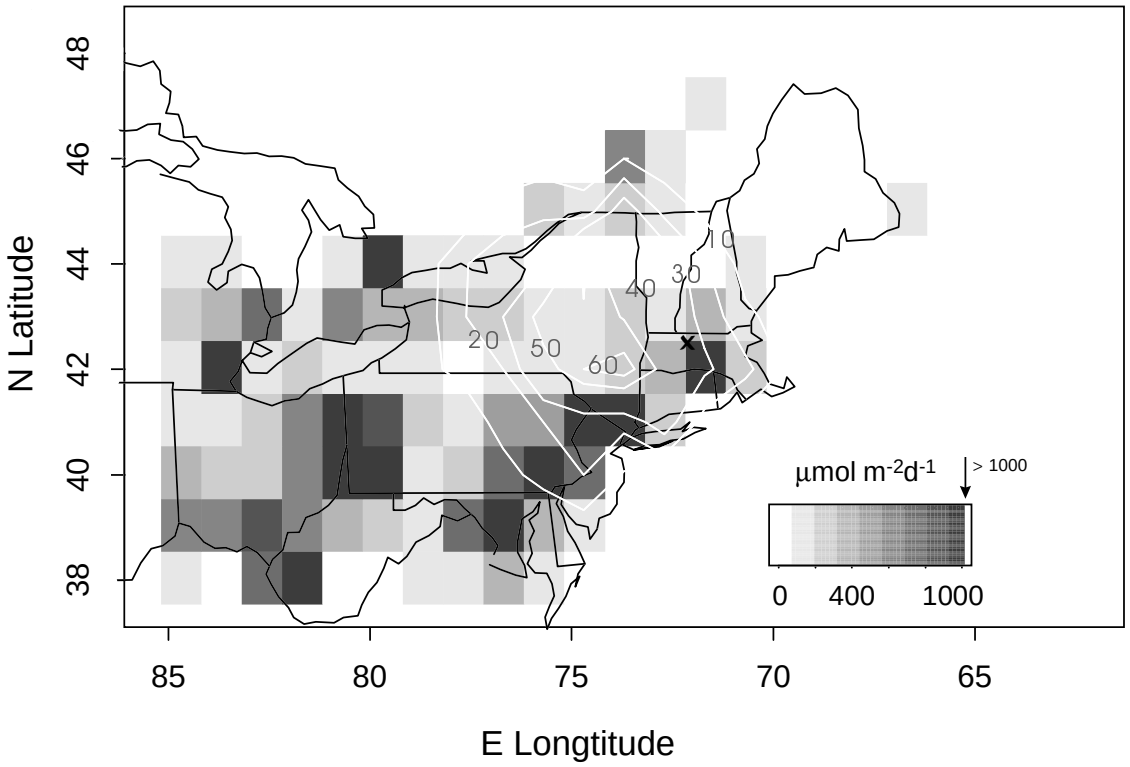
N Latitude
48
46
44
42
40
38
85
80
75
70
65
E Longtitude
10
20
30
40
50
60
μmol m-2d-1
> 1000
0
400
1000

Figure 1

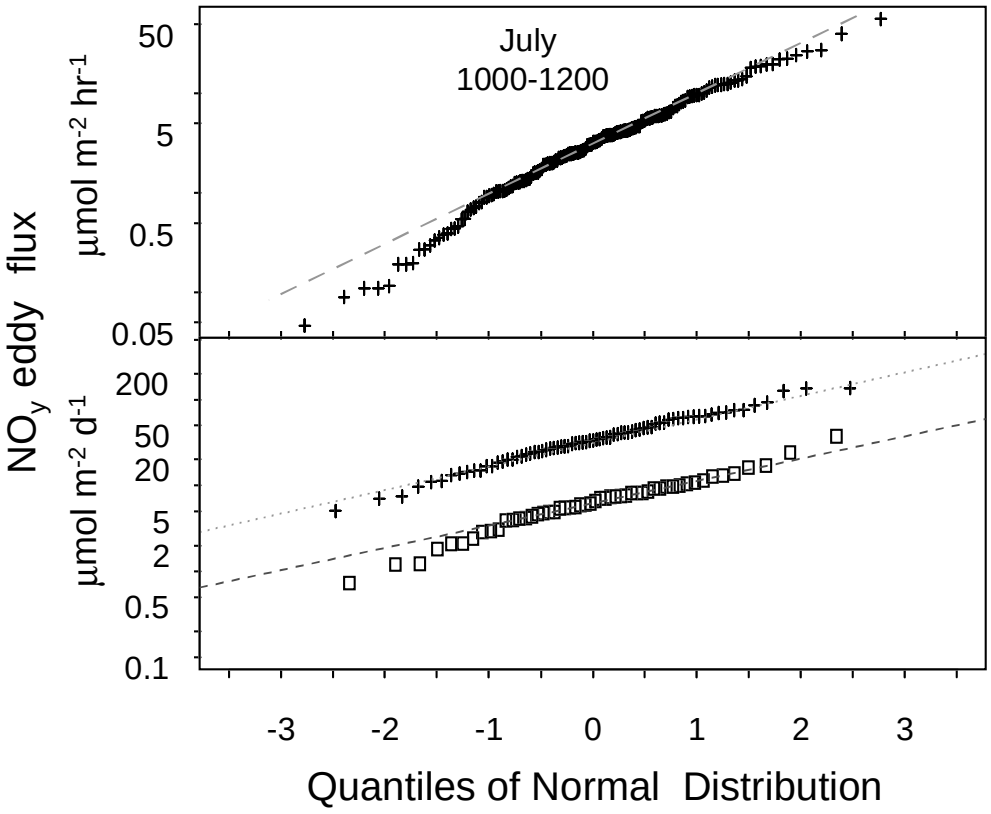
July
1000-1200
NO_y eddy flux
µmol m^{-2} hr^{-1}
µmol m^{-2} d^{-1}
50
5
0.5
0.05
200
50
20
5
2
0.5
0.1
-3
-2
-1
0
1
2
3
Quantiles of Normal Distribution

Figure 2

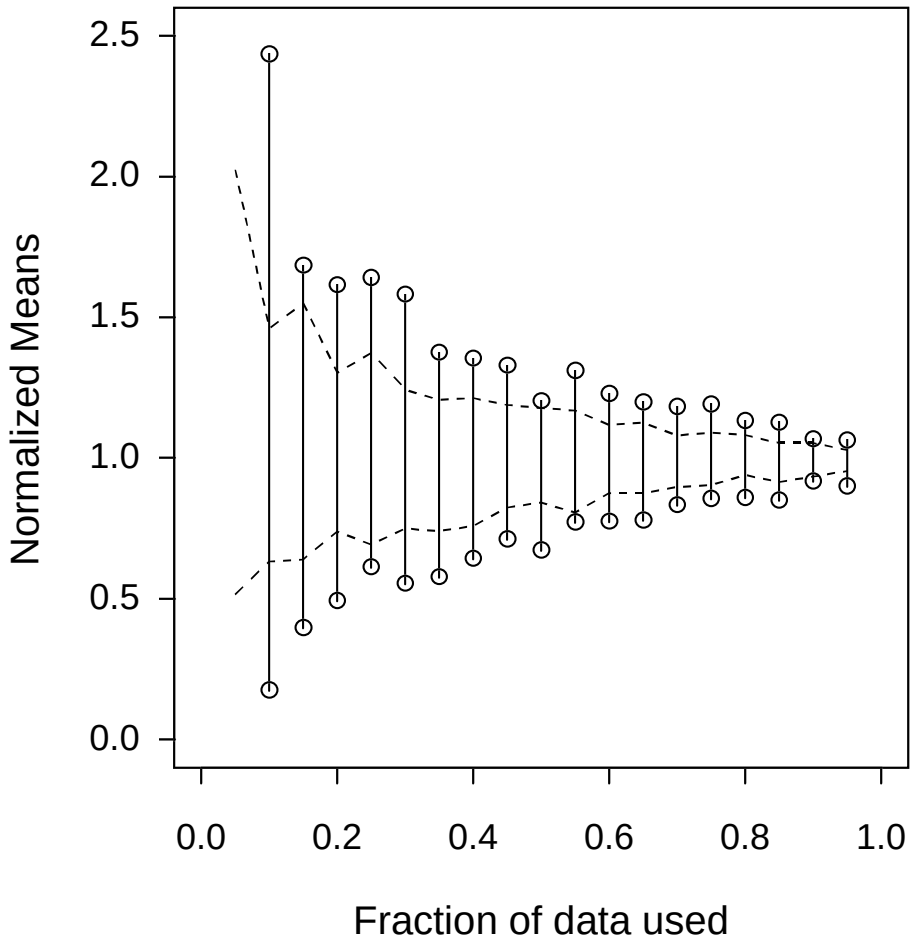
Normalized Means
2.5
2.0
1.5
1.0
0.5
0.0
0.0
0.2
0.4
0.6
0.8
1.0
Fraction of data used

Figure 3

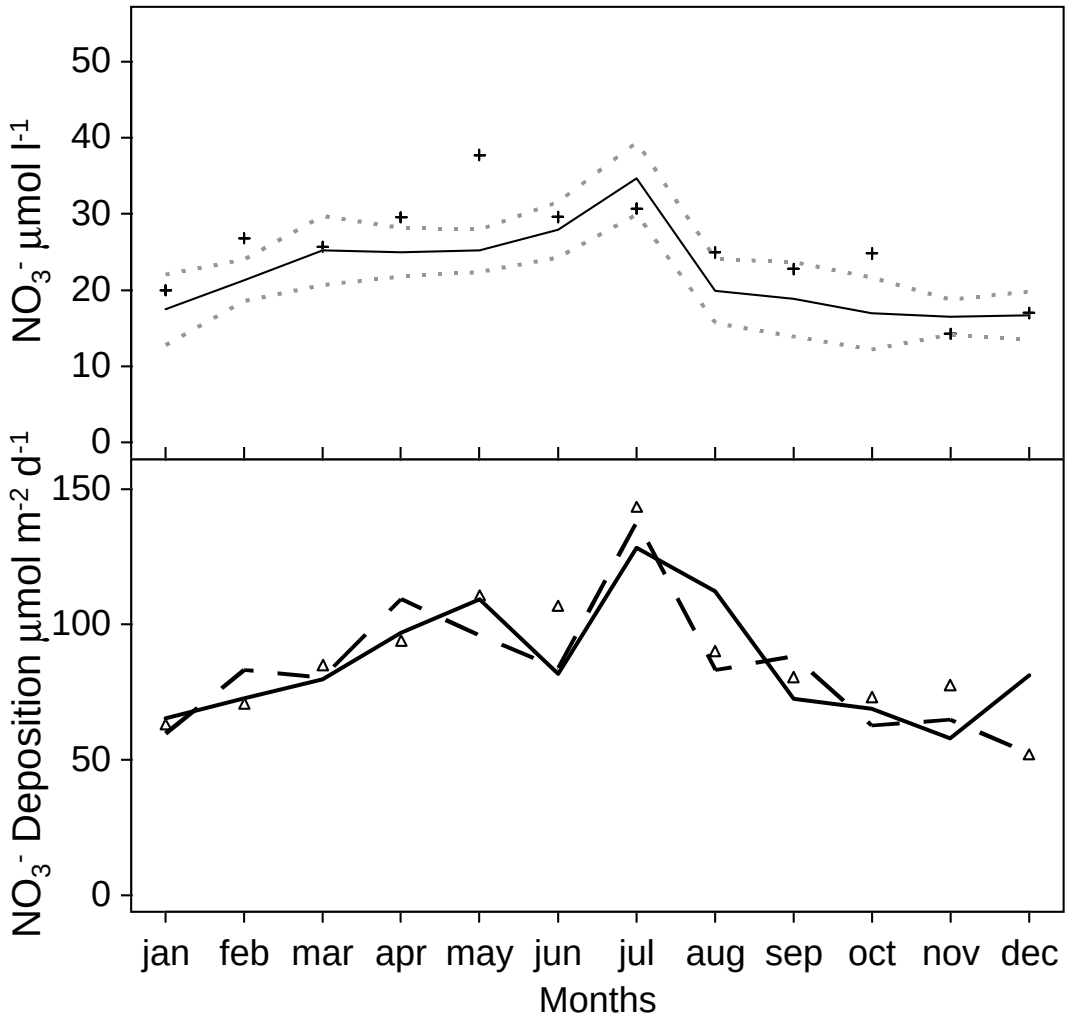
50
40
30
20
10
0
NO_3^- µmol l^{-1}
150
100
50
0
NO_3^- Deposition µmol m^{-2} d^{-1}
jan
feb
mar
apr
may
jun
jul
aug
sep
oct
nov
dec
Months

Figure 4

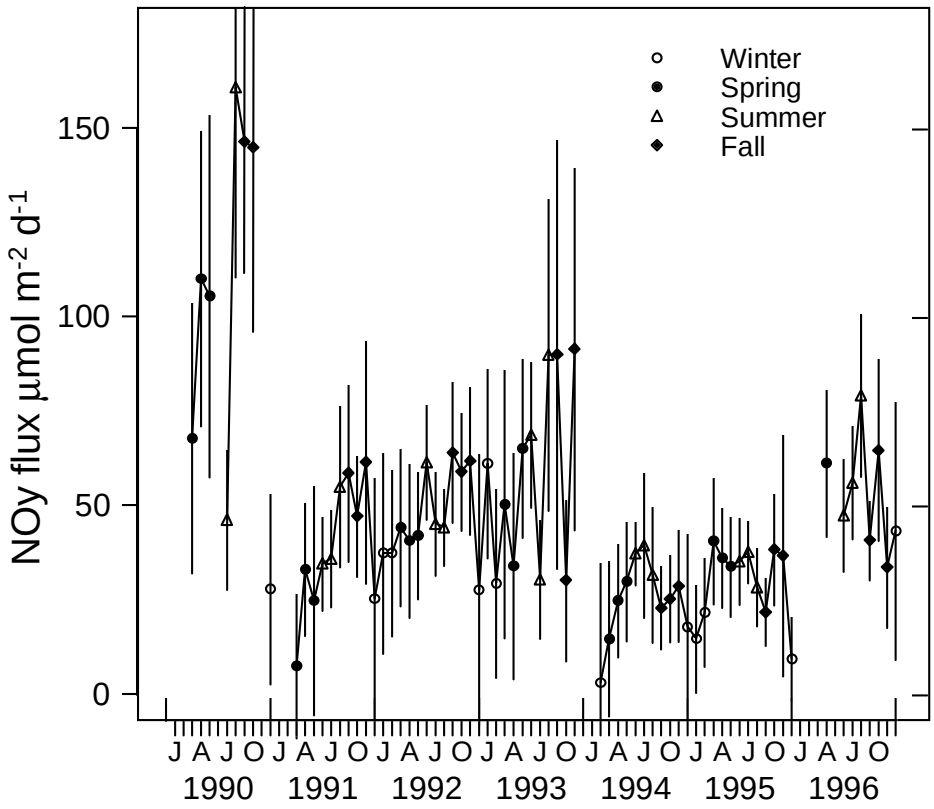
Winter
Spring
Summer
Fall
NOy flux µmol m-2 d-1
150
100
50
0
J A J O J A J O J A J O J A J O J A J O J A J O J A J O
1990 1991 1992 1993 1994 1995 1996

Figure 5

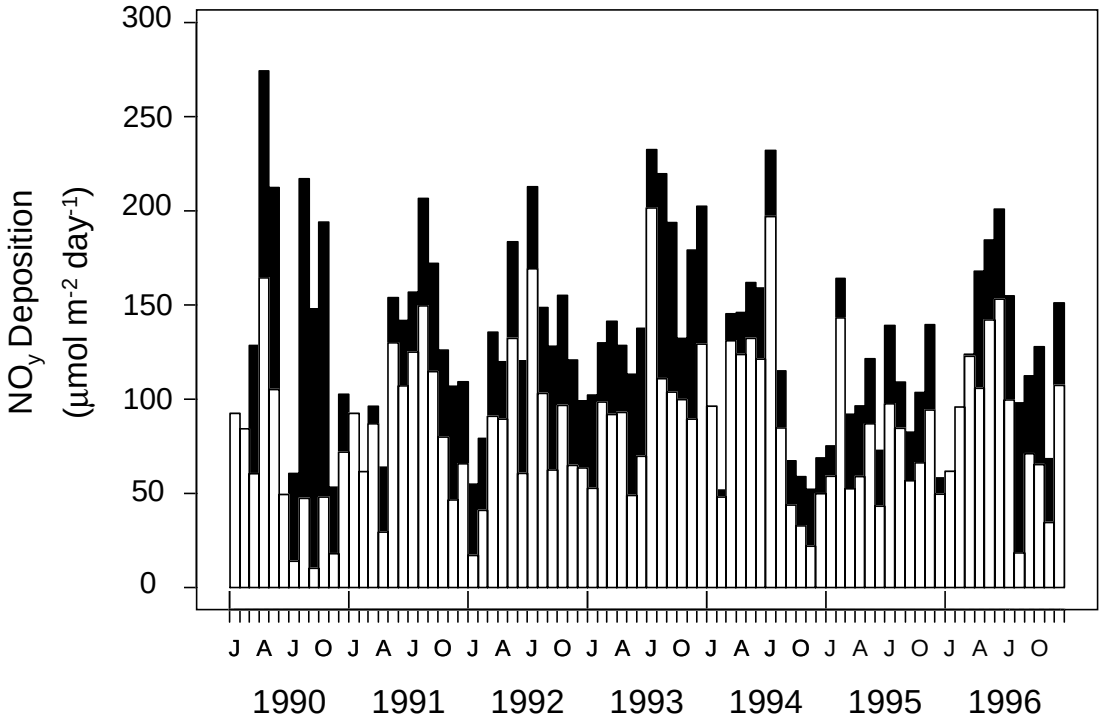
300
250
200
150
100
50
0
NOy Deposition
(µmol m-2 day-1)
J A J O J A J O J A J O J A J O J A J O J A J O J A J O
1990
1991
1992
1993
1994
1995
1996

Figure 6

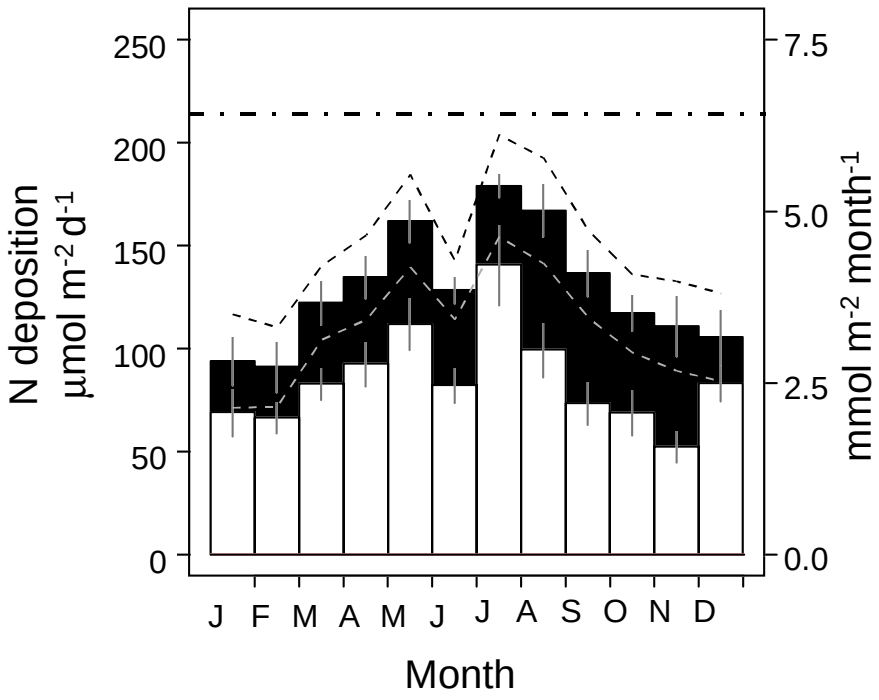
250
200
150
100
50
0
7.5
5.0
2.5
0.0
N deposition
µmol m-2 d-1
mmol m-2 month-1
J F M A M J J A S O N D
Month

Figure 7

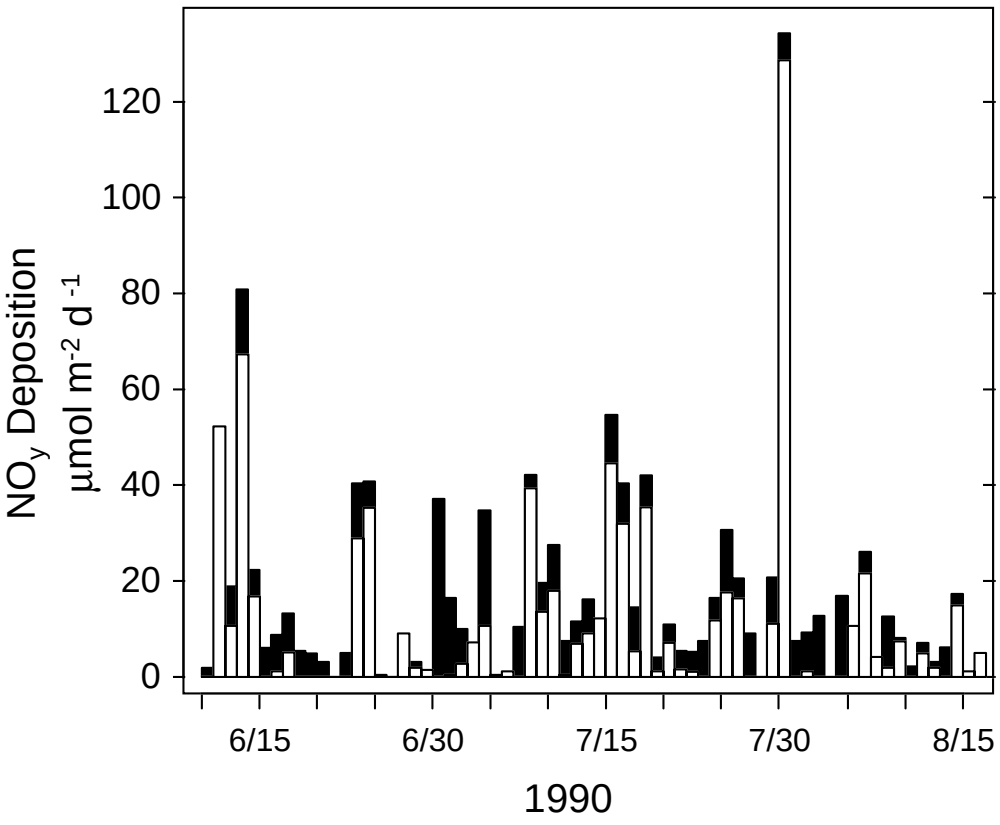
NOy Deposition
µmol m-2 d-1
0
20
40
60
80
100
120
6/15
6/30
7/15
7/30
8/15
1990

Figure 8

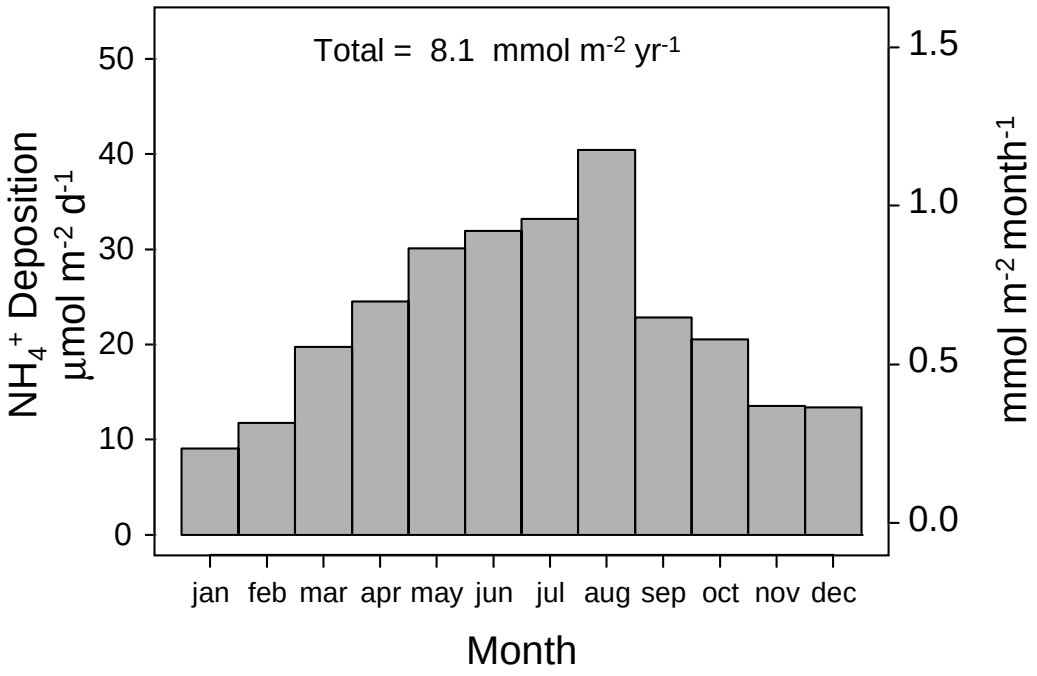
Total = 8.1 mmol m-2 yr-1
NH4+ Deposition
µmol m-2 d-1
mmol m-2 month-1
0
10
20
30
40
50
0.0
0.5
1.0
1.5
jan feb mar apr may jun jul aug sep oct nov dec
Month

Figure 9

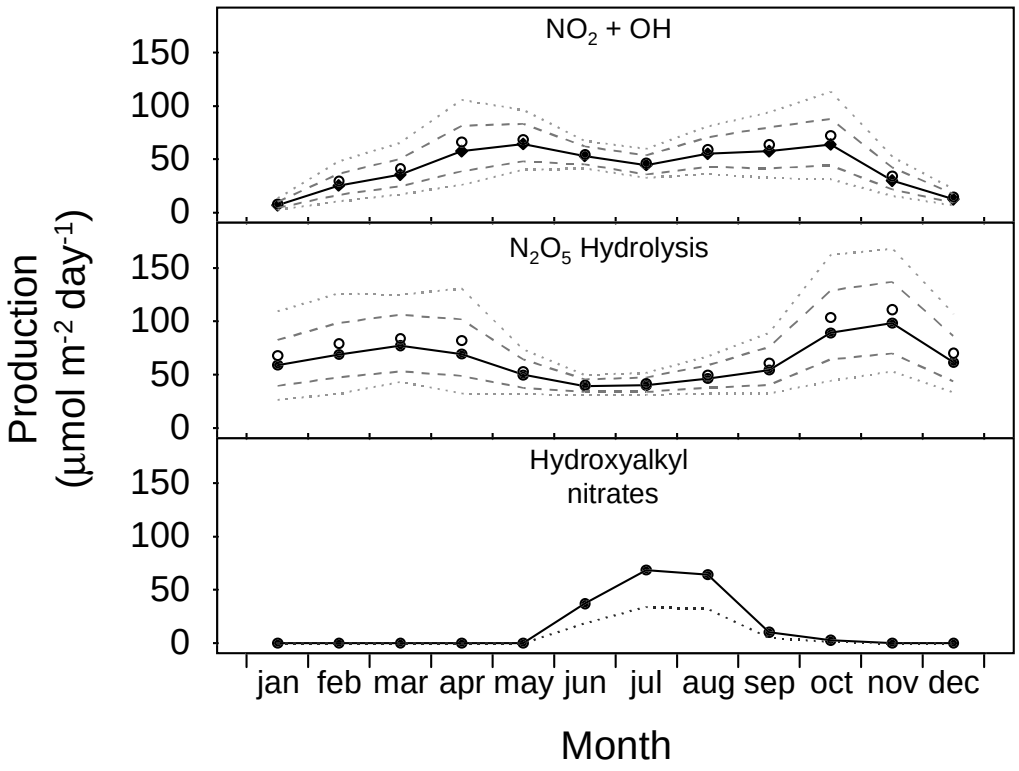
NO2 + OH
N2O5 Hydrolysis
Hydroxyalkyl
nitrates
150
100
50
0
Production
(µmol m-2 day-1)
jan feb mar apr may jun jul aug sep oct nov dec
Month

Figure 10

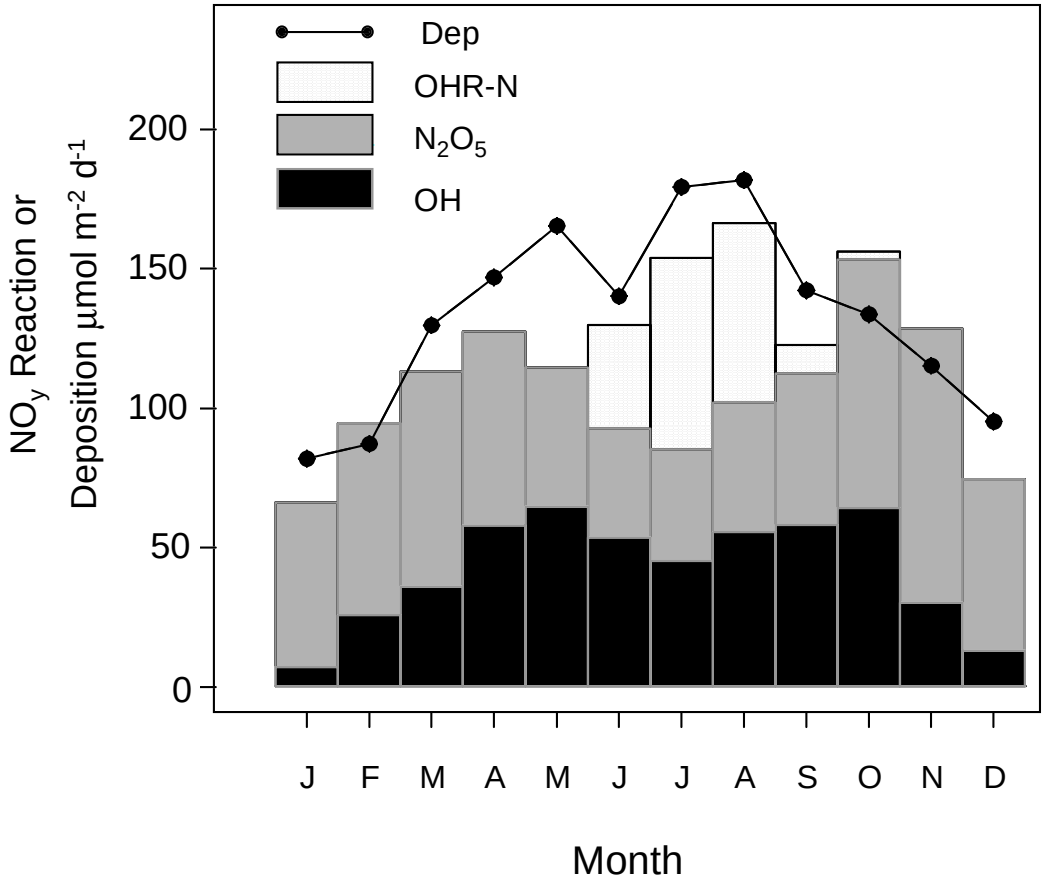
Dep
OHR-N
N_2O_5
OH
200
150
100
50
0
NO_y Reaction or
Deposition µmol m^{-2} d^{-1}
J F M A M J J A S O N D
Month

Figure 11

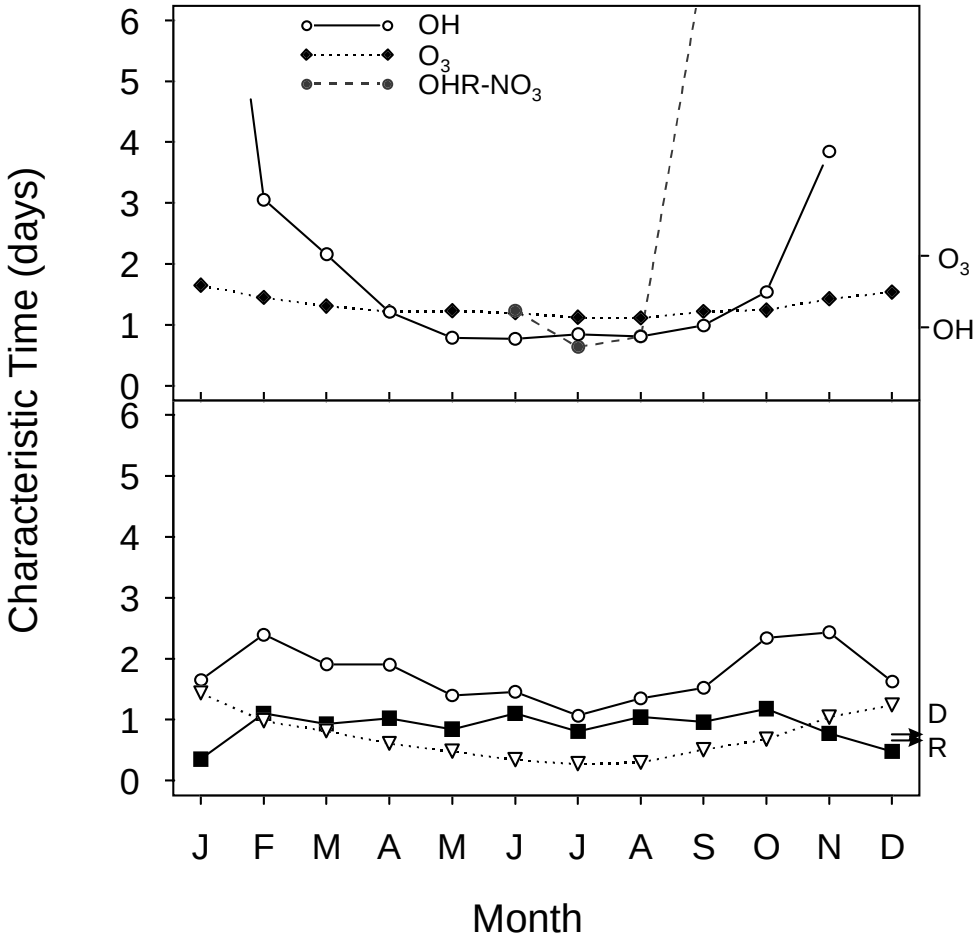
OH
O3
OHR-NO3
Characteristic Time (days)
O3
OH
D
R
J F M A M J J A S O N D
Month

Figure 12

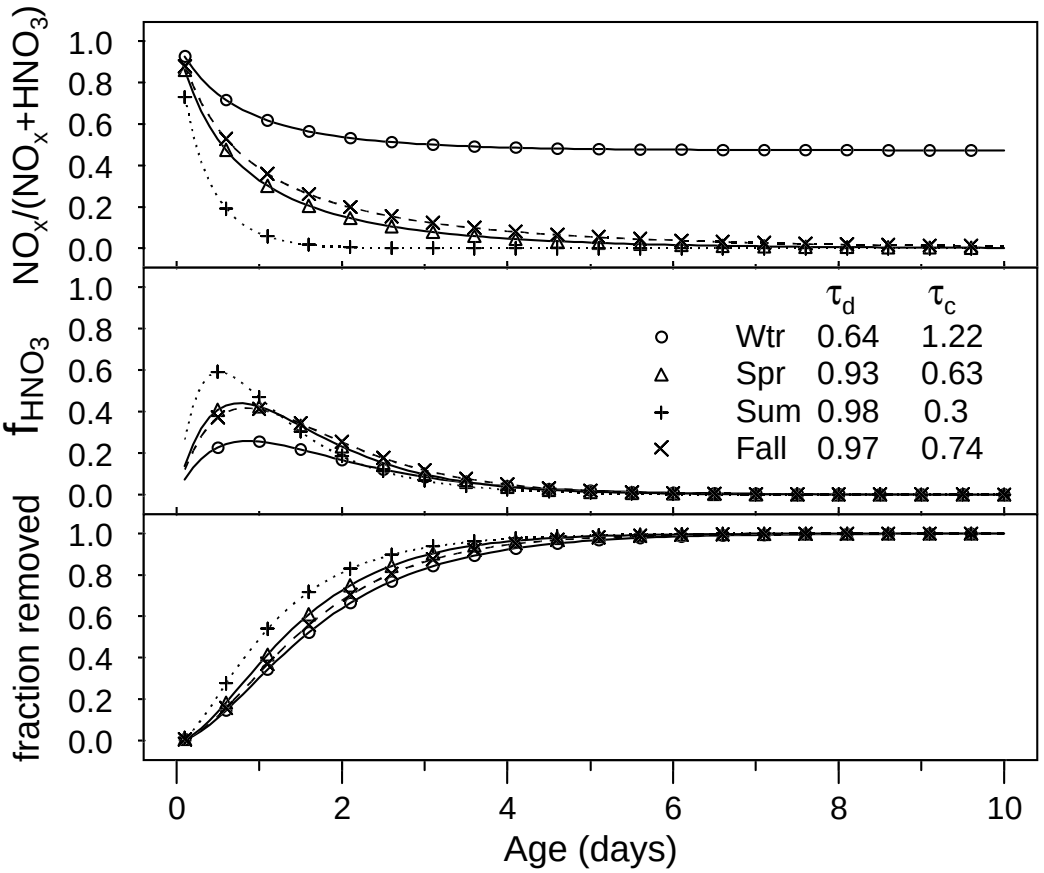
$NO_x/(NO_x+HNO_3)$
f_{HNO_3}
fraction removed
Age (days)
τ_d τ_c
Wtr 0.64 1.22
Spr 0.93 0.63
Sum 0.98 0.3
Fall 0.97 0.74

Figure 13